The Astrophysical Journal Letters, 992:L7 (9pp), 2025 October 10 https://doi.org/10.3847/2041-8213/ae08b7

Characterization of Two Cool Galaxy Outflow Candidates Using Mid-infrared Emission from Polycyclic Aromatic Hydrocarbons

Jessica Sutter[1], Karin Sandstrom[2], Ryan Chown[3], Oleg Egorov[4], Adam K. Leroy[3,5], Jérémy Chastenet[6], Alberto D. Bolatto[7], Thomas G. Williams[8], Daniel A. Dale[9], Amirnezam Amiri[10], Médéric Boquien[11], Yixian Cao[12], Simthembile Dlamini[13], Éric Emsellem[14,15], Hsi-An Pan[16], Debosmita Pathak[5,17], Hwihyun Kim[18], Ralf S. Klessen[19,20,21,22], Hannah Koziol[2], Erik Rosolowsky[23], Sumit K. Sarbadhicary[24], Eva Schinnerer[25], David A. Thilker[24], Leonardo Úbeda[26], and Tony Weinbeck[9]

[1] Whitman College, 345 Boyer Avenue, Walla Walla, WA 99362, USA; sutterjs@whitman.edu
[2] Department of Astronomy & Astrophysics, University of California, San Diego, 9500 Gilman Drive, La Jolla, CA 92093, USA
[3] Department of Astronomy, The Ohio State University, 140 West 18th Avenue, Columbus, OH 43210, USA
[4] Astronomisches Rechen-Institut, Zentrum für Astronomie der Universität Heidelberg, Mönchhofstraße 12-14, D-69120 Heidelberg, Germany
[5] Center for Cosmology and Astroparticle Physics (CCAPP), 191 West Woodruff Avenue, Columbus, OH 43210, USA
[6] Sterrenkundig Observatorium, Universiteit Gent, Krijgslaan 281 S9, B-9000 Gent, Belgium
[7] Department of Astronomy and Joint Space-Science Institute, University of Maryland, College Park, MD 20742, USA
[8] Sub-department of Astrophysics, Department of Physics, University of Oxford, Keble Road, Oxford OX1 3RH, UK
[9] Department of Physics and Astronomy, University of Wyoming, Laramie, WY 82071, USA
[10] Department of Physics, University of Arkansas, 226 Physics Building, 825 West Dickson Street, Fayetteville, AR 72701, USA
[11] Université Côte d'Azur, Observatoire de la Côte d'Azur, CNRS, Laboratoire Lagrange, 06000, Nice, France
[12] Max-Planck-Institut für Extraterrestrische Physik (MPE), Giessenbachstr. 1, D-85748 Garching, Germany
[13] Department of Astronomy, University of Cape Town, Rondebosch 7701, South Africa
[14] European Southern Observatory, Karl-Schwarzschild Straße 2, D-85748 Garching bei München, Germany
[15] Univ Lyon, Univ Lyon1, ENS de Lyon, CNRS, Centre de Recherche Astrophysique de Lyon UMR5574, F-69230 Saint-Genis-Laval, France
[16] Department of Physics, Tamkang University, No. 151, Yingzhuan Road, Tamsui District, New Taipei City 251301, Taiwan
[17] Department of Astronomy, Ohio State University, 180 W. 18th Avenue, Columbus, OH 43210, USA
[18] International Gemini Observatory/NSF NOIRLab, 950 N. Cherry Avenue, Tucson, AZ 85719, USA
[19] Universität Heidelberg, Zentrum für Astronomie, Institut für Theoretische Astrophysik, Albert-Ueberle-Str. 2, 69120 Heidelberg, Germany
[20] Universität Heidelberg, Interdisziplinäres Zentrum für Wissenschaftliches Rechnen, Im Neuenheimer Feld 225, 69120 Heidelberg, Germany
[21] Harvard-Smithsonian Center for Astrophysics, 60 Garden Street, Cambridge, MA 02138, USA
[22] Elizabeth S. and Richard M. Cashin Fellow at the Radcliffe Institute for Advanced Studies at Harvard University, 10 Garden Street, Cambridge, MA 02138, USA
[23] Dept. of Physics, University of Alberta, 4-183 CCIS, Edmonton, Alberta, T6G 2E1, Canada
[24] Department of Physics and Astronomy, The Johns Hopkins University, Baltimore, MD 21218, USA
[25] Max-Planck-Institut für Astronomie, Königstuhl 17, D-69117, Heidelberg, Germany
[26] Space Telescope Science Insititue, Baltimore, MD 21218, USA
Received 2025 July 23; revised 2025 September 13; accepted 2025 September 15; published 2025 October 3

Abstract

We characterize two candidate cool galactic outflows in two relatively low-mass, highly inclined Virgo cluster galaxies: NGC 4424 and NGC 4694. Previous analyses of observations using the Atacama Large Millimeter/submillimeter Array carbon monoxide (CO) line emission maps did not classify these sources as cool outflow hosts. Using new high-sensitivity, high-spatial-resolution, JWST mid-infrared photometry in the polycyclic aromatic hydrocarbon (PAH)–tracing F770W band, we identify extended structures present off of the stellar disk. The identified structures are bright in the MIRI F770W and F2100W bands, suggesting they include PAHs as well as other dust grains. As PAHs have been shown to be destroyed in hot, ionized gas, these structures are likely to be outflows of cool ($T \leqslant 10^4$ K) gas. This work represents an exciting possibility for using mid-infrared observations to identify and measure outflows in lower-mass, lower star formation galaxies.

Unified Astronomy Thesaurus concepts: Interstellar medium (847); Galaxies (573); Polycyclic aromatic hydrocarbons (1280); Infrared photometry (792)

1. Introduction

Outflows—gas and dust ejected from the disk of a galaxy—are an important factor in driving galaxy evolution and quenching. High star formation activity or an active galactic nucleus (AGN) can generate winds powerful enough to create outflows (T. M. Heckman 2002; A. C. Fabian 2012), contributing to the eventual suppression of star formation (see, e.g., S. Veilleux et al. 2020; T. A. Thompson & T. M. Heckman 2024). Outflows also enrich the gas in the circumgalactic and intracluster media. The exact composition, structure, and mass of outflowing material can provide important information about how galaxies and the surrounding medium evolve over time. Millimeter-wavelength observations have shown that these outflows can contain cool molecular gas (C. Cicone et al. 2014). As cool gas ($T \lesssim 10^4$ K (the temperatures at which hydrogen will be neutral, and therefore PAHs are most likely to be found; K. M. Sandstrom et al. 2012; B. S. Hensley et al. 2022; R. Chown et al. 2024) plays an essential role in forming new stars, its removal and recycling have major implications for galaxy evolution.

Cool outflows can carry small dust grains, including polycyclic aromatic hydrocarbons (PAHs), out of the host

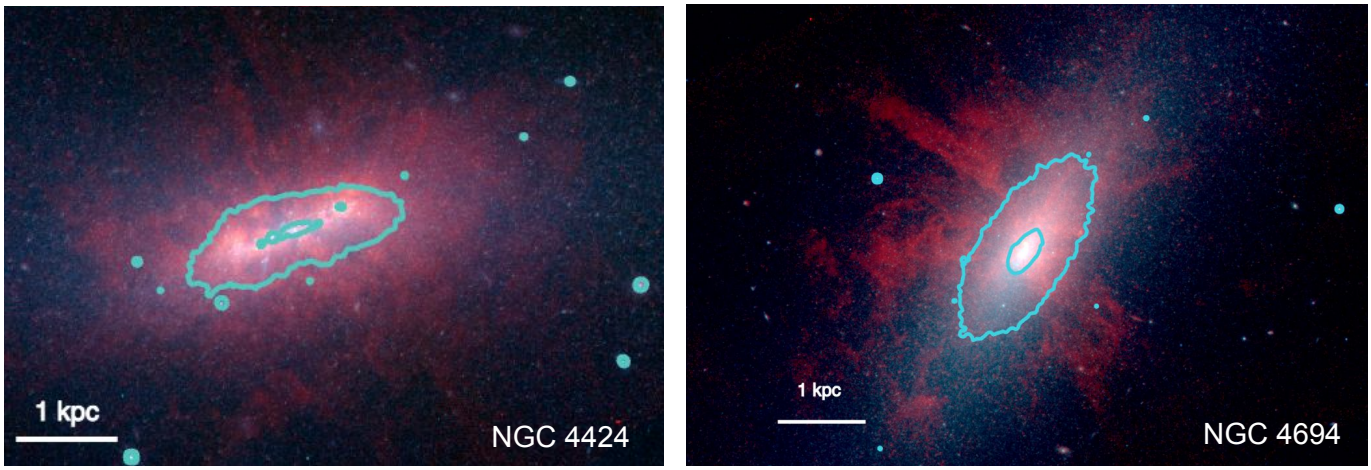

Figure 1. Three-color images of the two outflow candidate galaxies, NGC 4424 (left) and NGC 4694 (right). In both, red is F770W (PAH emission), green is F335M (stellar + PAH emission), and blue is F300M (stellar emission). Cyan contours represent the 10 MJy sr^{-1} and 2 MJy sr^{-1} in F300M, highlighting the location and extent of the stellar disk. The grayscale bar in the lower left of each image shows 1 kpc. North is up, and east is to the right in both images.

galaxy (C. W. Engelbracht et al. 2006; J. A. Irwin & S. C. Madden 2006; J. A. Irwin et al. 2007; A. McCormick et al. 2013). PAHs produce many near- and mid-infrared (MIR) emission features, which can be responsible for up to 20% of the IR emission from a galaxy (J. D. T. Smith et al. 2007), and have been shown to trace dense gas (R. Chown et al. 2025). The near-IR and MIR observations required to trace the small dust grains in these past studies were primarily made by the Spitzer Space Telescope, with additional observations from the Infrared Space Observatory and Akari. JWST provides an unprecedented opportunity to trace the PAHs and other dust grains in outflows and generally in extraplanar material at unprecedented sensitivity and spatial resolution (see, e.g., A. D. Bolatto et al. 2024; J. Chastenet et al. 2024; D. B. Fisher et al. 2025), improving on both the sensitivity and spatial resolution of Spitzer by a factor of ∼10.

We identify and characterize two candidate galactic-scale cool outflows detected in the MIR with JWST in galaxies NGC 4424 and NGC 4694. While finding PAHs in outflowing gas is not unusual (see, e.g., A. McCormick et al. 2013, who find extended PAH emission in 15 out of 16 galaxies with known outflows), it is rare that outflowing gas is primarily identified or characterized using PAH emission. Both galaxies are relatively low-mass ($\log_{10}M_\star/M_\odot \sim 9.9$, A. K. Leroy et al. 2019) Virgo Cluster occupants. While both galaxies were included in the work of S. K. Stuber et al. (2021), which used velocity profiles from Atacama Large Millimeter/submillimeter Array (ALMA) CO 2–1 maps of the 90 Physics at High Angular resolution in Nearby Galaxies (PHANGS)–ALMA galaxies to identify molecular outflows, neither were confirmed as an outflow host (see Section 4.1). The presence of outflowing gas is evident in the filamentary PAH emission detected in the MIR, which extends well beyond the stellar disk observed in the near-IR. As we only use photometry and no velocity measurements for this characterization, we cannot definitively confirm whether these structures are truly outflows. Because of this, we refer to the detected structures as "candidate" outflows throughout the Letter. Three-color images highlighting the differences in the stellar and dust disks of both NGC 4424 and NGC 4694 are displayed in Figure 1. Properties of both galaxies are listed in Table 1.

Table 1
Properties of Host Galaxies and the Outflow Candidates

Property	NGC 4424	NGC 4694
Distance (Mpc)	16.20	15.76
Inclination (deg)	58.2	60.7
Stellar Mass ($M_\odot$)	8.1×10^9	7.2×10^9
Position Angle (deg)	88	143
R_{25} (arcmin]	1.5	1.0
$\log_{10}M_\star$ ($M_\odot$)	9.9	9.9
$\mathrm{SFR}_{\mathrm{z0mgs}}$[a] ($M_\odot$ yr^{-1})	0.30	0.15
$\mathrm{SFR}_{\mathrm{MUSE}}$ ($M_\odot$ yr^{-1})	0.18	0.06
θ_{M87}[b] (deg)	3.11	4.58
Properties of Outflows		
Extent (kpc)	0.73–1.1	1.2–2.3
Estimated Gas Mass ($\log_{10}M_\odot$)	$7.11^{7.85}_{6.76}$	$6.37^{7.10}_{6.01}$
$\mathrm{F770W_{SS}}$/F2100W	1.45	1.38
Estimated $\dot{M}$ ($M_\odot$ yr^{-1})	$0.4^{+2.0}_{-0.3}$	$0.2^{+0.8}_{-0.15}$

Notes. Distances are from G. S. Anand et al. (2021); orientation parameters are from P. Lang et al. (2020), which used rotation curves to measure inclinations, position angles, and central R.A. and decl.; and the stellar masses and star formation rates are from A. K. Leroy et al. (2019). Outflow candidate properties were determined using the method described in Section 3.1 and the contours shown in Figures 2 and 3.
[a] Star formation rates from the $z = 0$ Multi-wavelength Galaxy Synthesis are global measurements, covering a larger area than the MUSE maps, which is why they are higher than the SFR values from MUSE.
[b] Angular separation from M87, i.e., the center of the Virgo Cluster, from S. Lee et al. (2022).

2. Outflow Candidates and Data

2.1. NGC 4424

NGC 4424, shown in Figure 2, is classified as a peculiar starburst galaxy due to the heart-shaped isophotes measured in the R band by J. R. Cortés et al. (2006). It is located near the edge of the Virgo Cluster (projected distance of 3.°11 or 880 kpc from M87; see θ_{M87} in Table 1) but has a projected distance of ∼1.°5 (420 kpc) from M49, another giant elliptical in Virgo. This suggests that NGC 4424 may be part of a smaller cluster currently in the process of merging into the larger Virgo Cluster (S. Mei et al. 2007). Optical studies of

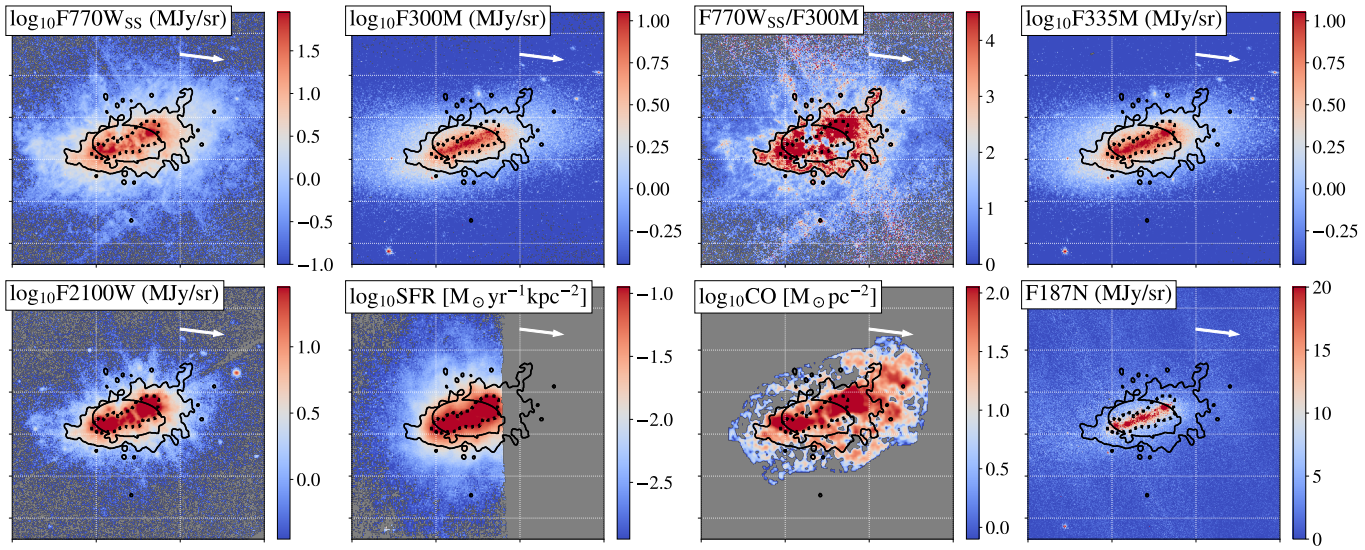

Figure 2. Multiwavelength images of NGC 4424. In each panel, the white arrow represents the direction toward M87, and the dashed black contour outlines areas where the SFR surface density exceeds 0.1 $M_{\odot}$ yr^{-1} kpc^{-2}; i.e., the Heckman number (T. M. Heckman 2002). The H I tail extends in the opposite direction as M87, opposite the white arrow, but is outside the field of view of these images so is not shown here. Solid black contours represent areas identified as outflows and used to estimate the outflow rates in Section 4.2. In all panels, north is up and east is to the right. Top row, left to right: F770W$_{SS}$, highlighting MIR PAH emission; F300M, showing the stellar disk; F770W$_{PAH}$/F300M, emphasizing the differences between the stellar disk and the extended PAH emission; and F335M, showing the lack of enhanced emission from small PAHs. Bottom row, left to right: F2100W, showing the emission from larger dust grains; SFR measured by extinction-corrected Hα from MUSE; CO (2–1) integrated intensity from ALMA; and F187N map, showing the lack of Paschen α emission in outflows. The MUSE coverage is incomplete, so only the area of the galaxy with coverage is shown.

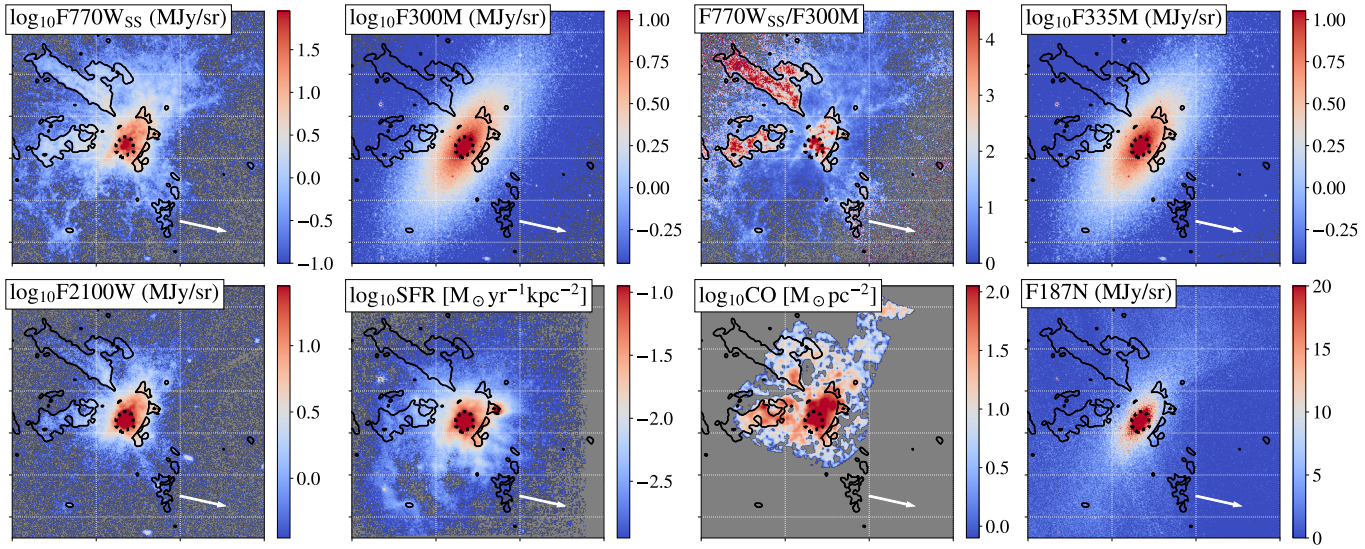

Figure 3. Same as Figure 2, but for NGC 4694. Similarly, emission in the MIR tracing dust is extended off the stellar plane. Similar to NGC 4424, the H I tail extends in the opposite direction as the arrow pointing toward M87 but is outside of the field of view of these images.

NGC 4424 have suggested the possibility of a past intermediate-mass merger based on asymmetries in the stellar disk (J. R. Cortés et al. 2006), along with an ionized gas outflow noted in the asymmetries of the [O III] velocity as well as an extended Hα tail noted in A. Boselli et al. (2018). Additional radio continuum measurements show two polarized cones, indicative of a nuclear outflow (B. Vollmer et al. 2013). Both these works suggest the origin of these outflows was a central starburst approximately 500 Myr ago, triggered by the past collisions. They support this claim through measurements of the velocity dispersion in the ionized gas outflows ratios of emission lines suggestive of a starburst (A. Boselli et al. 2018). This past starburst activity is likely the source of the filamentary PAH emission structures presented here. H I data show the presence of a tidally stripped tail (S. Lee et al. 2022).

2.2. NGC 4694

NGC 4694, shown in Figure 3, is a lenticular galaxy similarly located at the edge of the Virgo Cluster, far from M87 (projected distance of 4.°58 or 1.3 Mpc). While there is no clear evidence of past mergers, H I observations have detected the presence of a gas bridge connecting it to VCC2062, a nearby dwarf galaxy (U. Lisenfeld et al. 2016), while S. Lee et al. (2022) classify it as currently undergoing tidal stripping based on the shape and distribution of the H I tail. The M. P. Véron-Cetty & P. Véron (2010) catalog identifies

NGC 4694 as the host of an AGN, which could be the source of the presented outflow candidate.

2.3. James Webb Space Telescope Imaging

The two outflow candidates were identified based on unusual structures discerned from MIR observations obtained by JWST. Both of these galaxies are part of the PHANGS-JWST Cycle 2 Treasury (GO 3707, PI: A. Leroy; see the appendix in R. Chown et al. 2025), which mapped them in two MIRI and four NIRCam bands. The two MIRI bands are F770W (central wavelength 7.7 μm, width 1.95 μm, resolution 0.″27), which includes the 7.7 μm PAH feature and is therefore used to trace PAH emission, and F2100W (central wavelength 21.0 μm, width 4.58 μm, resolution 0.″67), which is dominated by stochastically heated small dust grains. The four NIRCam bands are F150W (central wavelength 1.5 μm, width 0.318 μm, resolution 0.″049), primarily tracing the stellar continuum; F187N (1.87 μm, 0.024 μm width resolution 0.″61), covering the Paschen α emission line; F300M (3.0 μm, 0.318 μm width, resolution 0.″097), primarily tracing warm, small dust grains and stellar continuum emission; and F335M (central wavelength 3.35 μm, 0.348 μm width angular resolution 0.″109), which includes the 3.3 μm PAH feature. For this work, we focus primarily on the MIRI bands, where the observed outflow is most prominent. We use the F300M band for comparison as it shows the location of the stellar disk. All JWST data were processed using `pjpipe`[27] (T. G. Williams et al. 2024), which supplements the official JWST pipeline. `pjpipe` modifies the official pipeline to suit observations of large extended sources through additional adjustments to the astrometric alignment and the background matching. As these images often have few point sources identified in the MIR, an additional alignment step is added to correct for small offsets that remain when using the standard pipeline. Additionally, as these images typically have large-scale diffuse emission from the source that fills the field, `pjpipe` replaces the `skymatch` algorithm used for background matching between MIRI tiles in the standard pipeline with a pixel-by-pixel method that takes into account the widespread signal that exists in the overlap regions. Finally, `pjpipe` adds an additional absolute flux calibration step called "anchoring" in which the images are matched to wider field-of-view archival images taken at similar wavelength from either IRAC or the Wide-field Infrared Survey Explorer to determine the true background values (see T. G. Williams et al. 2024 for more details). All MIRI observations have dedicated background images observed in parallel to the NIRCam observations, which are used to remove background signals during level two of the pipeline. To match the resolution between the different filters, we smooth all data to a common resolution of 0.″85, which corresponds to a physical resolution of $\sim$65 pc in both candidates. This has been shown to improve the signal-to-noise ratio in low-flux regions without a major loss to the high spatial sensitivity provided by JWST (T. G. Williams et al. 2024). The data were smoothed using the `stpsf` models and the method described in G. Aniano et al. (2011). With this smoothing method, the assumed 1σ sensitivities in each band are 0.13 MJy sr^{-1} for F770W, 0.27 MJy sr^{-1} for F2100W, 0.1 MJy sr^{-1} for F150W, 1 MJy sr^{-1} for F187N, 0.052 MJy sr^{-1} for F300M, and 0.050 MJy sr^{-1} for F335M.

[27] https://pjpipe.readthedocs.io/en/latest/

While the F770W filter is dominated by PAH and dust emission, in many sight lines, the Rayleigh–Jeans tail of stellar continuum emission contributes a significant fraction of the observed F770W intensity. To obtain the F770W intensity solely from dust and PAH emission, we subtract stellar continuum using the calibration from J. Sutter et al. (2024):

$$\mathrm{F770W_{SS}} = \mathrm{F770W} - 0.22 \times \mathrm{F300M}.$$

We do not remove any other underlying continuum, which would likely be from larger dust grains, as both PAHs and larger dust grains imply cooler gas in the outflows, so emission from these grains is of interest in our analysis. We use the F300M images to remove continuum instead of F150W due to persistent striping in F150W, which we have yet to model and remove and which can dominate the emission in this filter in low-signal-to-noise regions.

2.4. Multiwavelength Data

We use data from several archival data sets of these two sources. Specifically, we have optical integral field unit (IFU) data from the Multi-Unit Spectral Explorer (MUSE) on the Very Large Telescope obtained as part of programs 097.D-0408, PI: J. Anderson (NGC 4424), and 110.244E, PI: L. Cortese (NGC 4694); ALMA maps of the CO ($J = 2$–1) line obtained as part of PHANGS program (A. K. Leroy et al. 2021a, 2021b); and 21 cm H I maps from the Very Large Array Imaging of Virgo spirals in Atomic Gas (VIVA) survey (A. Chung et al. 2009). Together, these data provide a view of the stars and ionized gas (MUSE), the molecular gas (ALMA), and the neutral gas (VIVA). The MUSE data are used to measure the star formation rate (SFR) surface density, using the extinction-corrected Hα data and the method described in F. Belfiore et al. (2023), and are reduced using the method described in E. Emsellem et al. (2022).

3. Outflow Candidate Identification

The outflow candidates were both identified as part of routine quality assurance (QA) checks of all the PHANGS-JWST Cycle 2 Treasury sources. As part of the QA process, NIRCam and MIRI images are compared and overlaid to check for astrometry shifts across the images. During the completion of these checks for all 74 galaxies in the survey, NGC 4424 and NGC 4694 alone were identified as having clearly distinct structures in the near-IR bands, tracing primarily starlight and the MIR bands and tracing primarily dust emission. This check includes a step where ratio maps of the NIRCam and MIRI data are produced and examined, primarily for checking for astrometry shifts. The ratio maps showed elevated levels of dust emission perpendicular to the stellar disk, indicating the presence of an outflow. Only these two in the sample of 74 galaxies show these structures.

Based on these notes, further inspection of these two sources was performed, identifying the filamentary structures extending off of both sides of the disk. To isolate the pixels that are part of the filamentary structures, we use the ratio of the $\mathrm{F770W_{SS}}$ and F300M filters. This ratio is chosen as $\mathrm{F770W_{SS}}$ is our only tracer of PAH emission and F300M traces the stellar disk. We use F300M instead of the F150W NIRCam images due to prominent striping patterns in the F150W data that become the dominant signal at high radius and cause anomalously low values of the $\mathrm{F770W_{SS}}$/F150W value.

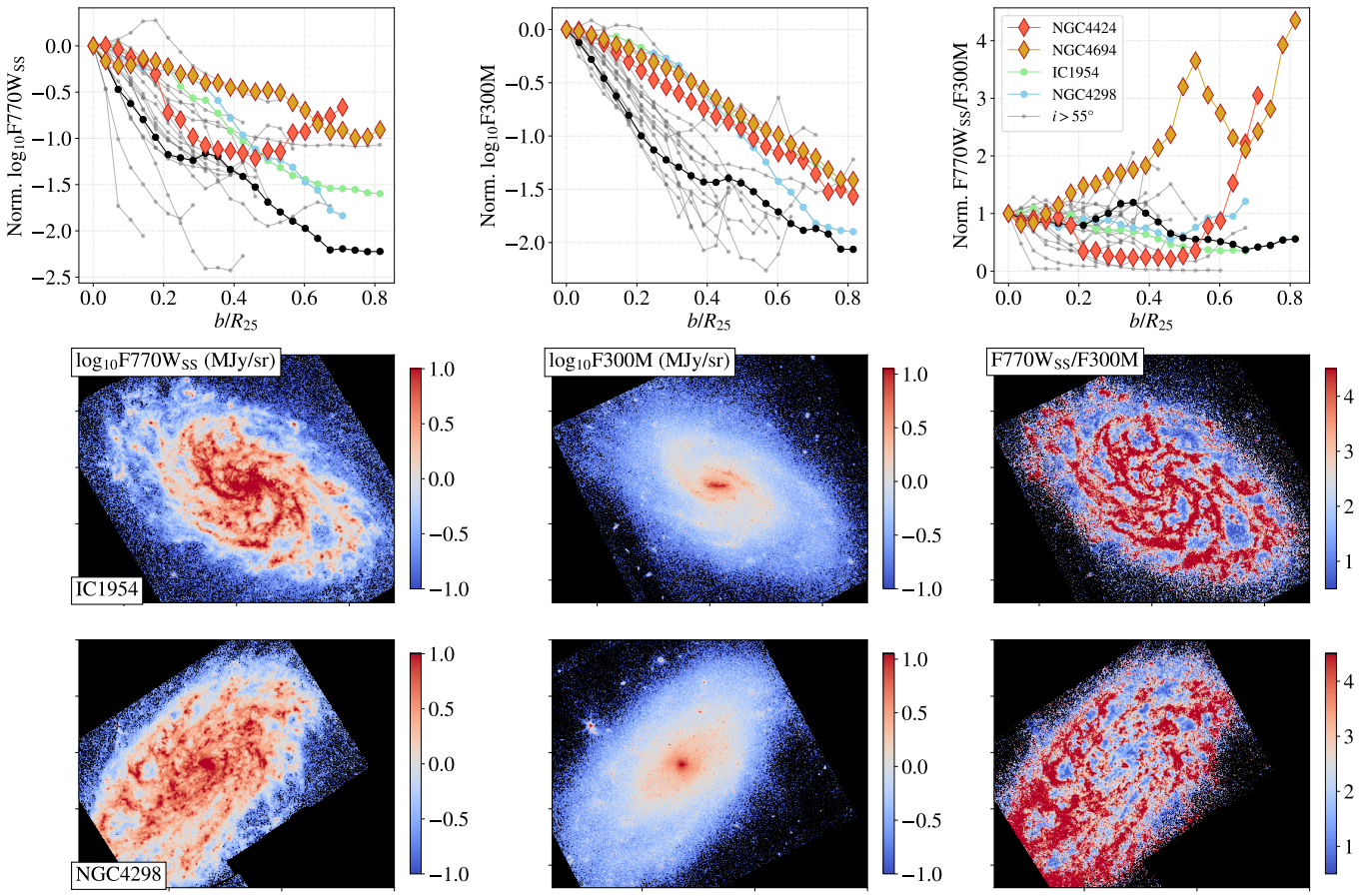

Figure 4. Top row: profiles of the median flux normalized to the central value, shown in the direction along the minor axis across the full image. The left panel shows the F770W$_{SS}$ data, the middle panel shows F300M tracing the stars, and the right panel shows the ratio of the two. The two outflow candidates are shown in red (NGC 4424) and yellow (NGC 4694), while two comparison galaxies of similar mass and inclination, IC 1954 and NGC 4298, are shown in green and blue, respectively. All 18 galaxies in the PHANGS sample with inclinations greater than 55° are also shown as gray lines, with the median of this comparison sample shown as a black line. Middle row: MIRI F770W$_{SS}$, NIRCam F300M, and the ratio of the two maps of the primary comparison galaxy IC 1954 on the same scales as Figures 2 and 3. Bottom row: same as previous, for comparison galaxy NGC 4298. For both comparison galaxies, the PAH emission (measured in F770W$_{SS}$) and starlight (measured by F300M) basically trace the same structures.

Contours encapsulating the filaments were produced by identifying all pixels with an F770W$_{SS}$/F300M value greater than twice the average F770W$_{SS}$/F300M value all pixels within the central $0.15R_{25}$ and a projected radius of greater than $0.15R_{25}$ to exclude the region used to find the central value. The value of 2× the central $0.15R_{25}$F770W$_{SS}$/F300M was determined using comparisons to the 18 additional galaxies included in the PHANGS-JWST Treasuries with $i > 55°$, shown in the top panels of Figure 4. The identified structures are outlined with black contours in Figures 2 and 3. Further details about the comparison sample are provided in the Appendix. Only the two outflow candidate host galaxies show F770W$_{SS}$/F300M reaching above twice the central ratio, indicating that this value is a good indicator of the unique conditions in cool outflows.

3.1. Distinguishing between Outflows and Tidal Stripping

Both NGC 4424 and NGC 4694 have been identified as galaxies experiencing ram pressure stripping based on 21 cm observations of 52 Virgo Cluster galaxies (S. Lee et al. 2022). Interestingly, NGC 4424 and NGC 4694 were the only two galaxies in this sample with H I tails classified as "atypical," where the predicted ram pressure would not be enough to produce the large extent of the observed tidal tail (S. Lee et al. 2022). With this finding in mind, we carefully consider whether our observations are indeed indicative of an outflow or are instead the PAH component of these stripped tails. The primary factor that indicates that we are observing outflowing gas, as opposed to stripped gas, is the presence of the structures above and below the stellar disk in both candidate galaxies, which would likely not be the case if gas were being stripped. These structures are approximately an order of magnitude smaller in extent than the detected stripped gas tails and do not appear to be associated with them (see Section 4.1 for further discussion).

To test whether these structures are signs of outflows or stripped gas, we compare our outflow candidates to other high-inclination galaxies in the PHANGS-JWST sample. We select the 18 galaxies in the PHANGS-JWST sample with inclinations greater than 55° and a wide enough field of view to see above and below the stellar disk.[28] The Appendix contains further details about all of the galaxies in the comparison sample, but to briefly summarize, this sample contains four additional Virgo Cluster galaxies, two galaxies with documented ram pressure stripping, and several galaxies currently undergoing tidal interactions with a nearby companion,

[28] NGC 3239 was also excluded from this analysis due to its irregular structure, producing the final list of 18 galaxies.

making it a representative sample of other potential methods for removing or perturbing gas in a galaxy besides outflows. Additionally, images of IC 1954 and NGC 4298 are shown in the lower panels of Figure 4 as representative examples of the full comparison sample due to their similar inclinations ($i \sim 57°$, $59°$) and field of view of the MIRI coverage reaching a similar height of the disk ($0.8 \times R_{25}$), so we can be certain that any similar outflow structures would be included in the observations. In Figure 4, we show images of IC 1954 and NGC 4298 in F770W$_{SS}$ and F300M, and the ratio of these two filters in the central (IC 1945) and lower (NGC 4298) panels. As with all the galaxies in our comparison sample, there are no clear PAH-bright components extending off the disk, and the F770W$_{SS}$ and F300M show similar structures.

We plot the normalized profiles of F770W$_{SS}$, F300M, and their ratio as a function of projected distance from the plane of the galaxy, b, for the two outflow hosts and all the galaxies in the comparison sample in the top panels of Figure 4. Each profile is normalized using the central value of the given intensity or ratio. While the comparison sample and the outflow candidates show similar exponentially decreasing trends in F300M, the profiles of the F770W$_{SS}$ data are significantly flatter in the two outflow candidates, indicating the presence of extended PAH emission off the plane of the galaxy. This difference in behavior is made clear in the top right panel of Figure 4, which shows F770W$_{SS}$/F300M as a function of distance from the plane. While the comparison galaxies either remain fairly flat or show decreasing trends in this ratio (see gray lines for individual galaxies, or black line for the median of the full comparison sample), the two outflow candidates display an increasing ratio with distance from the plane. This highlights the presence of PAH emission observed off the planes of these galaxies, tracing the outflowing gas.

4. Results

4.1. Comparison to Multiwavelength Data

4.1.1. JWST Photometry

The outflows are primarily detected in the F770W band, tracing PAHs, but are also visible in the F2100W images of both galaxies. This suggests that there are additional larger dust grains also being removed by these outflows. Notably, in both galaxies, the areas classified as outflows have a slightly higher average F770W$_{SS}$/F2100W than the stellar disks. This could indicate that the PAH/dust ratio is slightly lower in the star-forming main disk than in the outflowing gas but could also be due to differences in the radiation field heating the PAHs and dust in the disk compared to the outflowing gas, as a softer radiation field could still excite the PAHs without heating the dust as significantly, lowering the F2100W value (see, e.g., the models of B. T. Draine et al. 2014).

None of the NIRCam filters shows any sign of outflowing material in either galaxy. Notably, this includes the F335M filter, which includes the 3.3 μm PAH emission feature typically associated with smaller PAH molecules (B. T. Draine et al. 2021), and the F187N filter, which contains the Paschen α line, shown in the rightmost bottom panel of Figures 2 (NGC 4424) and 3 (NGC 4694). Previous studies of the 3.3 μm/7.7 μm ratio in a set of star-forming galaxies showed very low ($\sim$0.05) ratios across the full disks (J. Chastenet et al. 2023; H. Koziol 2025, in preparation), indicating that the 3.3 μm feature may simply be below the detection threshold of these observations. As the average surface brightness at F770W in the outflows was $\sim$1 MJy sr^{-1}, the expected F335M fluxes would be 0.05 MJy sr^{-1}, the 1σ limit for our observations (see T. G. Williams et al. 2024, Table 1). While we cannot rule out the presence of 3.35 μm emission, we can state that it is not enhanced in the outflow, suggesting at minimum a PAH population that is not dominated by the smallest PAHs. This matches the simulations described in H. M. Richie & E. E. Schneider (2025), which showed the smallest dust grains are less likely to survive in outflows. Similarly, the lack of detection in the F187N filter could be due to sensitivity limits of this filter.

4.1.2. MUSE IFU Observations

Both galaxies have partial coverage by the MUSE IFU. We examine the emission from several optical emission lines including Hα, [O III] 5007 Å, and [N II] 6584 Å. In both galaxies, these optical emission lines do show some extended emission off of the plane, which can be seen in the SFR maps in the lower middle panel of Figures 2 and 3. A. Boselli et al. (2018) also identified an ionized gas outflow from NGC 4424 but do not include NGC 4694 as an outflow host. These ionized gas outflows seem to be adjacent to, but not overlapping with, the cool outflows detected in the F770W band.

4.1.3. ALMA CO Observations

No outflows were detected in either galaxy in the work of S. K. Stuber et al. (2021), which classified outflows based on velocity profiles of two circular regions including the central 300 pc and 2000 pc from ALMA CO(2–1) mapping as well as *pv* maps along the major and minor axes. We compare the CO(2–1) intensity map to the MIRI F770W$_{SS}$ data and find similar structures across the stellar disk for both galaxies but do not detect CO throughout the full F770W-identified filaments. CO(2–1) is detected by ALMA in the region defined as the outflow in both sources, but for consistency, we use only the F770W$_{SS}$ derived gas masses in this work as $I_{CO(2-1)}$ falls below the sensitivity limits of these ALMA observations for the edges of the outflow structures.

4.1.4. VIVA H I 21 cm Maps

Multiple papers have described the extended 21 cm emission detected around NGC 4424 and NGC 4694 (A. Chung et al. 2007; A. Sorgho et al. 2017; S. Lee et al. 2022). These observations show an $\sim$18 kpc long tail extending from only the southeast side of NGC 4424 and a $\sim$30 kpc tail from only the southwest side of NGC 4694. These tails are an order of magnitude larger than the outflows described here (0.73–2.3 kpc, Table 1), and the VIVA H I maps have angular resolutions of 20″ and are therefore not of high enough angular resolution for us to determine if the filaments outlined in the black contours in Figures 2 and 3 are detected at 21 cm.

4.2. Estimating Mass Outflow Rates in the MIR

Using the high sensitivity of the JWST-MIRI observations, we provide an order-of-magnitude estimate of the mass outflow rates in these two galaxies. To do so, we first convert the F770W$_{SS}$ map to a gas surface density map using the method described by R. Chown et al. (2025). We use the

individual galaxy best-fit relationships to predict $I_{CO(2-1)}$ in the CO bright part of the disks:

$$\log_{10} I_{CO(2-1)} = m \times \log_{10}(\mathrm{F770W_{ss}} - x_0) + b,$$

with m, b, x_0 = 0.816, 0.406, 0.480 for NGC 4424 and 0.821, 0.294, 0.360 for NGC 4694. We use the predicted $I_{CO(2-1)}$ instead of the ALMA maps to leverage the higher sensitivity of the MIRI observations, detecting even the low surface brightness edges of the outflow filaments that fall below the sensitivity of the ALMA observations, as discussed in Section 4.1.

With these F770W$_{SS}$-scaled gas maps, the total mass of the outflows is estimated using the contours defined in Section 3. We convert from predicted F770W$_{SS}$-predicted $I_{CO(2-1)}$ to a gas mass using a single α_{CO} of 0.8 $M_\odot$ pc^{-2}(K km/s)$^{-1}$, which is often used for starburst galaxies and outflows, and an R_{21} of 0.65 (A. D. Bolatto et al. 2013; S. K. Stuber et al. 2021). It should be noted that while the method of converting from MIRI photometry to a total gas mass has inherit scatter, the largest uncertainty in this calculation will come from the choice of α_{CO}, which could change the calculated gas mass by up to a factor of 4. Assuming a maximum and minimum α_{CO} of the Milky Way α_{CO} = 4.35 $M_\odot$ pc^{-2}(K km/s)$^{-1}$ and the optically thin limit of α_{CO} = 0.35 $M_\odot$ pc^{-2}(K km/s)$^{-1}$, respectively (both from A. D. Bolatto et al. 2013), we get values for the gas mass of NGC 4424: $\log_{10} M\,[M_\odot] = 7.11^{7.85}_{6.76}$ and NGC 4694: $\log_{10} M\,[M_\odot] = 6.37^{7.10}_{6.01}$.

The mass outflow rate is given by

$$\dot{M} = \frac{M \times v}{l},$$

where v is the velocity of the outflow, M is the gas mass of the outflow (as calculated above), and l is the vertical extent of the outflow assuming a relatively constant density. Examining the moment 1 maps of the ALMA data described in Section 2, we find velocities of 13 km s^{-1} for NGC 4424 and 39 km s^{-1} for NGC 4694. Assuming the maximal case that these velocities are exactly perpendicular to the plane of each galaxy yields a total velocity of 25 km s^{-1} for NGC 4424 and 80 km s^{-1} for NGC 4694. It should be noted that less than half the pixels within the outflows have strong enough CO detections for a robust measurement of the velocity making these measurements highly uncertain. If we instead assume a typical outflow velocity for galaxies of a similar SFR from S. K. Stuber et al. (2021), we would expect outflow velocities of ∼100–130 km s^{-1}, although none of the galaxies within the sample of confirmed outflows have an SFR as low as NGC 4694. Additional measurements of the ionized gas outflow in NGC 4424 found it to have a velocity of 500 km s^{-1}, much higher than either the velocity measured from the CO emission or the outflows measured in S. K. Stuber et al. (2021). This could be due to the ∼3× larger radius of the ionized gas outflow than the radii of the outflows we present here. Based on these measurements, we assume a velocity of $v = 80 \pm 20$ km s^{-1} to span the measured and deprojected velocity of NGC 4694 and the velocities of the lowest SFR outflows presented in S. K. Stuber et al. (2021).

l is measured using the largest radial extent of the red contours shown in Figures 2 and 3 and is found to be between 1 and 2 kpc in both sources. Properties of the outflows are listed in Table 1. As we do not know the exact geometry of the outflows, we do not correct for inclination, so l is the length of the outflows as projected on the sky. Using this method, we find the mass outflow rate of NGC 4424 is $\sim 0.4^{+2.0}_{-0.3}\ M_\odot\ \mathrm{yr}^{-1}$ and NGC 4694 is $\sim 0.2^{+0.8}_{-0.15}\ M_\odot\ \mathrm{yr}^{-1}$. These mass outflow rates are close to what would be expected for a mass loading factor ($\dot{M}$/SFR) of ∼unity, matching the average value found in S. K. Stuber et al. (2021), though these galaxies have both SFR and $\dot{M}$ about 1 order of magnitude lower than the typical value of 3 $M_\odot\ \mathrm{yr}^{-1}$ for the identified outflow hosts in that paper.

5. Conclusions

In this Letter, we have shown how MIRI observations can be used to characterize cool outflowing gas in two galaxies: NGC 4424 and NGC 4694. These outflow candidates were measured by comparing the relatively smooth stellar disk to the clearly extended PAH and dust disk. Both of these galaxies are small ($\log_{10} M_\star/M_\odot = 9.9$) and highly inclined ($i > 55°$), making our observing angle ideal for seeing the outflowing dust and gas, and have some signs of additional ionized gas outflows detected in optical emission lines (A. Boselli et al. 2018). The outflowing gas in both sources has slightly elevated F770W$_{SS}$/F2100W compared to their disks, either signaling increased PAH fraction or changes to the radiation field heating the dust. While cool gas outflows have been detected in low-mass galaxies before (e.g., SMC, NGC 1569, NGC 55, NGC 5253; A. McCormick et al. 2013), the low surface brightness of the outflowing gas has made it difficult to observe the lower-mass, cool outflows in smaller galaxies at larger distances. The new IR observations from JWST provide the link between the dust and gas in these outflows and the ability to resolve the structures present in the outflowing gas.

This work shows that MIR observations with JWST hold the potential for discovery of galaxy-scale outflows in highly inclined sources where gas kinematics are poorly suited for outflow detection. This result demonstrates the power of using PAH-dominated MIR imaging with JWST to trace gas in galaxies (A. K. Leroy et al. 2023; R. Chown et al. 2025), opening a new window for studying low-mass outflows that would be undetected even with ALMA. This work signals the potential discovery space for finding dusty outflows in lower-mass galaxies.

Acknowledgments

The authors would like to thank the anonymous referee for careful consideration of this Letter and the detailed feedback that improved the analysis. H.A.P. acknowledges support from the National Science and Technology Council of Taiwan under grant 113-2112-M-032-014-MY3. J.C. acknowledges funding from the Belgian Science Policy Office (BELSPO) through the PRODEX project "JWST/MIRI Science exploitation" (C4000142239). M.B. acknowledges support from the ANID BASAL project FB210003. This work was supported by the French government through the France 2030 investment plan managed by the National Research Agency (ANR), as part of the Initiative of Excellence of Université Côte d'Azur under

reference number ANR-15-IDEX-01. O.E. acknowledges funding from the Deutsche Forschungsgemeinschaft (DFG, German Research Foundation)—project-ID 541068876.

This work has been carried out as part of the PHANGS collaboration. This work is based on observations made with the NASA/ESA/CSA JWST. The data were obtained from the Mikulski Archive for Space Telescopes at the Space Telescope Science Institute, which is operated by the Association of Universities for Research in Astronomy, Inc., under NASA contract NAS 5-03127 for JWST. These observations are associated with programs 2107 and 3707. The specific observations analyzed can be accessed via doi:10.17909/a2tt-kt68.

This work is also based on observations collected at the European Southern Observatory under ESO programs: 097.D-0408 (PI: J. Anderson) and 110.244E (PI: L. Cortese)

This Letter makes use of the following ALMA data: ADS/JAO.ALMA#2017.1.00886.L. ALMA is a partnership of ESO (representing its member states), NSF (USA), and NINS (Japan), together with NRC (Canada), NSC and ASIAA (Taiwan), and KASI (Republic of Korea), in cooperation with the Republic of Chile. The Joint ALMA Observatory is operated by ESO, AUI/NRAO, and NAOJ. The National Radio Astronomy Observatory is a facility of the National Science Foundation operated under cooperative agreement by Associated Universities, Inc.

Facilities: HST (STIS), Swift (XRT and UVOT), AAVSO, CTIO:1.3 m, CTIO:1.5 m, CXO.

Software: astropy (Astropy Collaboration et al. 2013, 2018).

Appendix
Comparison Sample Properties

In this appendix, we provide a brief summary of the properties of the galaxies in the comparison sample. The galaxies in this sample are all part of the PHANGS-JWST Cycle 2 Treasury Program and were selected primarily due to their high inclinations ($i < 55°$). The galaxies in this sample are used to exemplify how ram pressure stripping or recent gravitational interactions alone cannot produce the elevated off-plane PAH/starlight ratios observed in our two outflow candidate galaxies. It is therefore essential we consider the environment and recent history of each galaxy in the comparison sample. Importantly, nearly all of the galaxies in this sample are members of larger galaxy groups, as specified in the group membership column of Table 2, with four Virgo Cluster galaxies. Two of the Virgo Cluster members also have documented ram pressure stripping: NGC 4569 (A. Boselli et al. 2016) and NGC 4654 (Y. Sofue et al. 2003). Two in the comparison sample are currently undergoing tidal interactions with a nearby companion (NGC 4907 and NGC 4298), and NGC 4826 recently merged with an SMC-like companion (A. Smercina et al. 2023). One has documented inflowing gas (NGC 4536 P. da Silva & F. Combes 2024), and another has an extended UV disk (NGC 2090 D. A. Thilker et al. 2007). Despite this wide range of environmental influences, none in our comparison sample shows the same elevated PAH to stellar emission off the plane of the disk as our two outflow host candidate galaxies.

Table 2
Properties of Comparison Sample Galaxies

Galaxy	i (deg)	D (Mpc)	$\log_{10}M_\star$	$\log_{10}$SFR	Group Membership	Tidal Tail?
IC 1954	57.1	12.8	9.7	−0.44	LGG093	⋯
NGC 1546	70.3	17.7	10.4	−0.08	Dorado	⋯
NGC 1559	65.4	19.4	10.4	0.58	Dorado	⋯
NGC 1792	65.1	16.2	10.6	0.57	NGC 1808 Group	⋯
NGC 1809	57.6	20.0	9.8	0.76	⋯	⋯
NGC 2090	64.5	11.7	10.0	−0.39	⋯	⋯
NGC 2903	66.8	10.0	10.6	0.49	NGC 2903 Group	⋯
NGC 3137	70.3	16.4	9.9	−0.31	LGG189	⋯
NGC 3511	75.1	13.9	10.0	−0.09	⋯	⋯
NGC 3521	68.8	13.2	11.0	0.57	⋯	⋯
NGC 4298	59.2	14.9	10.0	−0.34	Virgo	⋯
NGC 4536	66.0	16.3	10.4	0.54	Virgo	⋯
NGC 4569	70.0	15.8	10.8	0.12	Virgo	✓
NGC 4654	55.6	22.0	10.6	0.58	Virgo	✓
NGC 4731	64.0	13.3	9.5	−0.22	LGG314	⋯
NGC 4781	59.0	11.3	9.6	−0.32	LGG307	⋯
NGC 4826	59.1	4.4	10.2	−0.70	⋯	⋯
NGC 4951	70.2	15.0	9.8	−0.45	LGG314	⋯

Note. Properties of the 18 comparison galaxies, selected from the PHANGS-JWST data. Comparison galaxies are selected based on their inclinations ($i > 55°$) and the extent of the JWST coverage above and below the stellar plane. Inclination (i) and distance (D) are from G. S. Anand et al. (2021), and $M_\star$ and SFR are from A. K. Leroy et al. (2019). Galaxy cluster membership is from the R. B. Tully (2015) catalog. Galaxies with an identified tidal tail from S. Lee et al. (2022) are marked with a ✓. Primary comparison galaxies are listed in bold.

ORCID iDs

Jessica Sutter https://orcid.org/0000-0002-9183-8102
Karin Sandstrom https://orcid.org/0000-0002-4378-8534
Ryan Chown https://orcid.org/0000-0001-8241-7704
Oleg Egorov https://orcid.org/0000-0002-4755-118X
Adam K. Leroy https://orcid.org/0000-0002-2545-1700
Jérémy Chastenet https://orcid.org/0000-0002-5235-5589
Alberto D. Bolatto https://orcid.org/0000-0002-5480-5686
Thomas G. Williams https://orcid.org/0000-0002-0012-2142
Daniel A. Dale https://orcid.org/0000-0002-5782-9093
Amirnezam Amiri https://orcid.org/0000-0002-8553-1964
Médéric Boquien https://orcid.org/0000-0003-0946-6176
Yixian Cao https://orcid.org/0000-0001-5301-1326
Simthembile Dlamini https://orcid.org/0000-0002-2885-6172
Éric Emsellem https://orcid.org/0000-0002-6155-7166
Hsi-An Pan https://orcid.org/0000-0002-1370-6964
Debosmita Pathak https://orcid.org/0000-0003-2721-487X
Hwihyun Kim https://orcid.org/0000-0003-4770-688X
Ralf S. Klessen https://orcid.org/0000-0002-0560-3172
Hannah Koziol https://orcid.org/0009-0001-5949-1524
Erik Rosolowsky https://orcid.org/0000-0002-5204-2259
Sumit K. Sarbadhicary https://orcid.org/0000-0002-4781-7291
Eva Schinnerer https://orcid.org/0000-0002-3933-7677
David A. Thilker https://orcid.org/0000-0002-8528-7340
Leonardo Úbeda https://orcid.org/0000-0001-7130-2880
Tony Weinbeck https://orcid.org/0009-0005-8923-558X

References

Anand, G. S., Lee, J. C., Van Dyk, S. D., et al. 2021, MNRAS, 501, 3621
Aniano, G., Draine, B. T., Gordon, K. D., & Sandstrom, K. 2011, PASP, 123, 1218
Astropy Collaboration, Price-Whelan, A. M., Sipőcz, B. M., et al. 2018, AJ, 156, 123
Astropy Collaboration, Robitaille, T. P., Tollerud, E. J., et al. 2013, A&A, 558, A33
Belfiore, F., Leroy, A. K., Sun, J., et al. 2023, A&A, 670, A67
Bolatto, A. D., Levy, R. C., Tarantino, E., et al. 2024, ApJ, 967, 63
Bolatto, A. D., Wolfire, M., & Leroy, A. K. 2013, ARA&A, 51, 207
Boselli, A., Cuillandre, J. C., Fossati, M., et al. 2016, A&A, 587, A68
Boselli, A., Fossati, M., Consolandi, G., et al. 2018, A&A, 620, A164
Chastenet, J., De Looze, I., Relaño, M., et al. 2024, A&A, 690, A348
Chastenet, J., Sutter, J., Sandstrom, K., et al. 2023, ApJL, 944, L12
Chown, R., Leroy, A. K., Sandstrom, K., et al. 2025, ApJ, 983, 64
Chown, R., Sidhu, A., Peeters, E., et al. 2024, A&A, 685, A75
Chung, A., van Gorkom, J. H., Kenney, J. D. P., Crowl, H., & Vollmer, B. 2009, AJ, 138, 1741
Chung, A., van Gorkom, J. H., Kenney, J. D. P., & Vollmer, B. 2007, ApJL, 659, L115
Cicone, C., Maiolino, R., Sturm, E., et al. 2014, A&A, 562, A21
Cortés, J. R., Kenney, J. D. P., & Hardy, E. 2006, AJ, 131, 747
da Silva, P., & Combes, F. 2024, A&A, 691, A58
Draine, B. T., Aniano, G., Krause, O., et al. 2014, ApJ, 780, 172
Draine, B. T., Li, A., Hensley, B. S., et al. 2021, ApJ, 917, 3
Emsellem, E., Schinnerer, E., Santoro, F., et al. 2022, A&A, 659, A191
Engelbracht, C. W., Kundurthy, P., Gordon, K. D., et al. 2006, ApJL, 642, L127
Fabian, A. C. 2012, ARA&A, 50, 455
Fisher, D. B., Bolatto, A. D., Chisholm, J., et al. 2025, MNRAS, 538, 3068
Heckman, T. M. 2002, in ASP Conf. Ser. 254, Extragalactic Gas at Low Redshift, ed. J. S. Mulchaey & J. T. Stocke (San Francisco, CA: ASP), 292
Hensley, B. S., Murray, C. E., & Dodici, M. 2022, ApJ, 929, 23
Irwin, J. A., Kennedy, H., Parkin, T., & Madden, S. 2007, A&A, 474, 461
Irwin, J. A., & Madden, S. C. 2006, A&A, 445, 123
Lang, P., Meidt, S. E., Rosolowsky, E., et al. 2020, ApJ, 897, 122
Lee, S., Sheen, Y.-K., Yoon, H., Jaffé, Y., & Chung, A. 2022, MNRAS, 517, 2912
Leroy, A. K., Hughes, A., Liu, D., et al. 2021a, ApJS, 255, 19
Leroy, A. K., Sandstrom, K., Rosolowsky, E., et al. 2023, ApJL, 944, L9
Leroy, A. K., Sandstrom, K. M., Lang, D., et al. 2019, ApJS, 244, 24
Leroy, A. K., Schinnerer, E., Hughes, A., et al. 2021b, ApJS, 257, 43
Lisenfeld, U., Braine, J., Duc, P. A., et al. 2016, A&A, 590, A92
McCormick, A., Veilleux, S., & Rupke, D. S. N. 2013, ApJ, 774, 126
Mei, S., Blakeslee, J. P., Côté, P., et al. 2007, ApJ, 655, 144
Richie, H. M., & Schneider, E. E. 2025, arXiv:2505.11734
Sandstrom, K. M., Bolatto, A. D., Bot, C., et al. 2012, ApJ, 744, 20
Smercina, A., Bell, E. F., Price, P. A., et al. 2023, ApJL, 949, L37
Smith, J. D. T., Draine, B. T., Dale, D. A., et al. 2007, ApJ, 656, 770
Sofue, Y., Koda, J., Nakanishi, H., & Onodera, S. 2003, PASJ, 55, 59
Sorgho, A., Hess, K., Carignan, C., & Oosterloo, T. A. 2017, MNRAS, 464, 530
Stuber, S. K., Saito, T., Schinnerer, E., et al. 2021, A&A, 653, A172
Sutter, J., Sandstrom, K., Chastenet, J., et al. 2024, ApJ, 971, 178
Thilker, D. A., Bianchi, L., Meurer, G., et al. 2007, ApJS, 173, 538
Thompson, T. A., & Heckman, T. M. 2024, ARA&A, 62, 529
Tully, R. B. 2015, AJ, 149, 171
Veilleux, S., Maiolino, R., Bolatto, A. D., & Aalto, S. 2020, A&ARv, 28, 2
Véron-Cetty, M. P., & Véron, P. 2010, A&A, 518, A10
Vollmer, B., Soida, M., Beck, R., et al. 2013, A&A, 553, A116
Williams, T. G., Lee, J. C., Larson, K. L., et al. 2024, ApJS, 273, 13